INSTITUTE OF PHYSICS PUBLISHING JOURNAL OF PHYSICS: CONDENSED MATTER

J. Phys.: Condens. Matter **14** (2002) R145–R167 PII: S0953-8984(02)21853-6

TOPICAL REVIEW

STM studies of single-walled carbon nanotubes

Teri W Odom, Jin-Lin Huang and Charles M Lieber[1]

Harvard University, Cambridge, MA 02138, USA

E-mail: cml@cmliris.harvard.edu

Received 6 August 2001, in final form 15 January 2002
Published 1 February 2002
Online at stacks.iop.org/JPhysCM/14/R145

Abstract

This topical review summarizes scanning tunneling microscopy investigations of the electronic properties of single-walled carbon nanotubes (SWNTs). First, the unique relationship between the atomic structure and electronic properties of SWNTs is reviewed. Second, the one-dimensional electronic band structure of SWNTs is introduced, and a comparison of tunneling spectroscopy to tight-binding calculations is presented. Third, localized structures in nanotubes, such as intramolecular junctions and ends, are addressed. Fourth, quantum size effects in SWNTs are discussed. Lastly, the effects of external perturbations, specifically magnetic impurities, on the low energy properties of metallic SWNTs are discussed. Prospects for future research directions are considered.

Carbon nanotubes have attracted considerable attention from both scientific and technological communities. This interest is not surprising in light of their promise to exhibit exceptional physical properties that may be exploited in areas from advanced composites to nanoelectronics [1–3]. Experimental studies have shown that carbon nanotubes are the stiffest known material [4, 5] and buckle elastically under large bending or compressive strains [5,6]. These mechanical characteristics suggest that nanotubes have potential for super-strong composites, and could be unique force transducers to the molecular world. Moreover, the remarkable electronic properties of carbon nanotubes offer great intellectual challenges and the potential for novel applications. For example, theoretical calculations first predicted that single-walled carbon nanotubes (SWNTs) could exhibit either metallic or semiconducting behavior depending only on diameter and helicity [7–9]. This ability to display fundamentally distinct electronic properties without changing the local bonding, which was experimentally demonstrated through atomically resolved scanning tunneling microscopy (STM) measurements [10, 11], sets nanotubes apart from all other nanowire materials [12, 13].

Scanning tunneling microscopy and spectroscopy (STS) have been exploited to interrogate the electronic properties of individual carbon nanotubes and SWNTs on the surfaces of ropes. This review will describe a broad range of STM studies, drawn primarily from the authors'

[1] Author to whom any correspondence should be addressed.

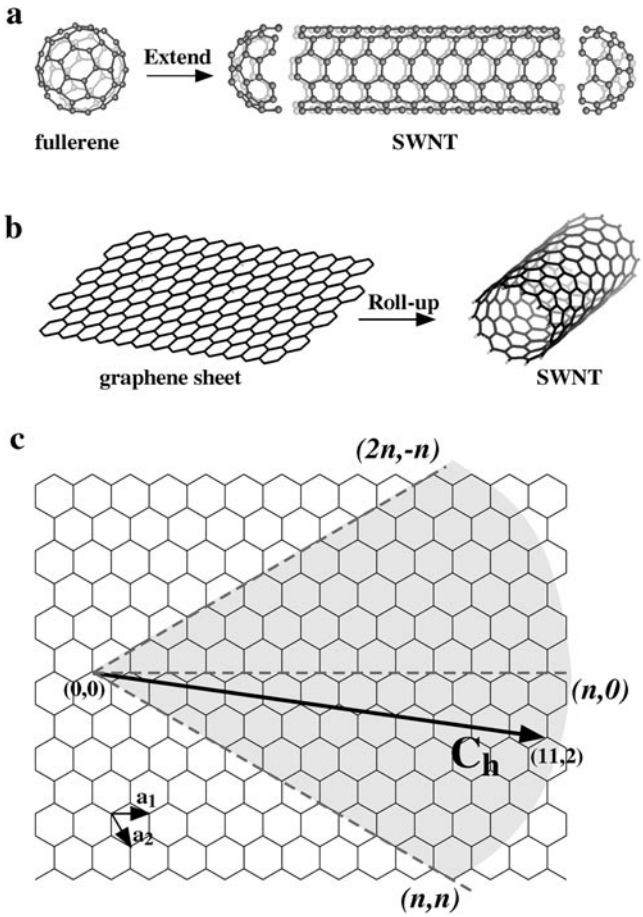

Figure 1. Schemes that represent a single-walled carbon nanotube: (*a*) extension in 1D of a fullerence molecular cluster. C_{60} can be extended into two end caps of a nanotube 0.7 nm in diameter. (*b*) Strip of a graphene sheet rolled up seamlessly into a hollow cylinder. (*c*) 2D graphene sheet illustrating lattice vectors $\boldsymbol{a}_1$ and $\boldsymbol{a}_2$, and the roll-up vector $\boldsymbol{C}_h = n\boldsymbol{a}_1 + m\boldsymbol{a}_2$. The limiting, achiral cases of $(n, 0)$ zigzag and (n, n) armchair are indicated with dashed lines. The shaded region between (n, n) and $(2n, -n)$ directions represents the area of unique (n, m) indices. The diagram is constructed for $(n, m) = (11, 2)$.

laboratory, addressing the unique electronic properties of nanotubes. First, the relationship between the atomic structure and electronic properties of SWNTs is reviewed. Second, the SWNT electronic band structure and comparison of the tunneling spectroscopy to tight-binding calculations are discussed. Third, the experimental and theoretical investigations of localized structures, such as intramolecular junctions and ends are described. Fourth, the effects of quantum size effects in shortened nanotubes are discussed. Finally, the effects of external perturbations, namely magnetic impurities, on metallic SWNTs are addressed. Prospects for future research are discussed.

1. Introduction

A SWNT can be viewed as an extended, fullerene molecular cluster or as a strip cut from an infinite graphene sheet rolled up to form a tube (figure 1). Major characteristics of their

electronic properties can be built up from Hückel-type models using p(π) atomic orbitals. The roll-up vector $\boldsymbol{C}_h$ uniquely characterizing a nanotube may be defined as a linear combination of the graphene lattice vectors $\boldsymbol{a}_1$ and $\boldsymbol{a}_2$:

$$\boldsymbol{C}_h = n\boldsymbol{a}_1 + m\boldsymbol{a}_2 \equiv (n, m) \tag{1}$$

where n and m are integers. $\boldsymbol{C}_h$ connects crystallographically equivalent sites on the graphene sheet. The nanotube diameter is simply C_h/π. Symmetry considerations constrain the chiral angle of a SWNT to one-sixth of the graphene sheet, where $0^\circ \leqslant |\theta| \leqslant 30^\circ$ (figure 1(c)). By convention, the chiral angle is measured from the zigzag $(n, 0)$ and either armchair $(n, n)/(2n, -n)$ direction, and is defined as negative between $(n, 0)$ and (n, n).

Electronic band structure calculations predict that the (n, m) indices determine whether a SWNT will exhibit metallic or semiconducting behavior [7–9]. To understand this ability to exhibit distinct electronic properties within an all-carbon, sp^2 hybridized network, it is instructive to consider the two-dimensional (2D) energy dispersion of graphite. Graphite is a semi-metal or zero-gap semiconductor whose valence and conduction bands touch at two inequivalent wavevectors $\boldsymbol{K}$ and $\boldsymbol{K}'$ and are degenerate at six k_F points. As a finite piece of the 2D graphene sheet is rolled up to form a one-dimensional (1D) tube, the periodic boundary conditions imposed by $\boldsymbol{C}_h$ can be used to enumerate the allowed 1D subbands—the quantized states resulting from radial confinement—as follows:

$$\boldsymbol{C}_h \cdot \boldsymbol{k} = 2\pi q \tag{2}$$

where q is an integer. If one of these allowed subbands passes through one of the $\boldsymbol{K}$ points, the nanotube will be metallic, and otherwise semiconducting. Thus to first order, zigzag $(n, 0)$ or chiral (n, m) SWNTs are metallic when $(n-m)/3$ is an integer, and otherwise semiconducting. In addition, the energy gaps of the semiconducting tubes are helicity-independent and should depend inversely on diameter [7–9].

The above discussion is based on the first order (π-only) approximation of the graphene band structure and neglects the curved nature of the nanotube. Theory has predicted that the finite curvature of the tubes leads to mixing of the π/σ bonding and π^*/σ^* anti-bonding orbitals in carbon, and can modify the above picture in two ways. First, finite curvature reduces the overlap between adjacent p(π) orbitals, and thereby causes k_F to shift from $\boldsymbol{K}$ in a $(n, 0)$ or (n, m) metallic tube. Second, curvature also causes the graphene band crossing (k_F) to shift away from the $\boldsymbol{K}$ point. Both effects can thus produce small gaps in $(n, 0)$ and (n, m) metallic tubes with the magnitude of the gap depending inversely with the square of the diameter [7, 14]. (n, n) armchair tubes, however, are expected to be truly metallic since k_F remains on the subband of the nanotube [15].

Away from the $\boldsymbol{K}$ point, signature features in the density of states (DOS) of a material appear at the band edges, and are commonly referred to as van Hove singularities (VHS). These singularities characterize the dimensionality of a system. In three dimensions, VHS are kinks due to the increased degeneracy of the available phase space, while in two dimensions the VHS appear as stepwise discontinuities with increasing energy. Unique to 1D systems, the VHS are manifest as peaks. Hence, SWNTs and other 1D materials are expected to exhibit spikes in their DOS due to the 1D nature of their band structure.

2. Structure and electronic properties of SWNTs

2.1. Historical background

Atomically resolved images of *in situ* vapor-deposited multi-walled carbon nanotubes (MWNTs) were first reported by Ge and Sattler [16]. Bias-dependent imaging [17] and STS investigations [18] of independently characterized arc generated MWNTs suggested

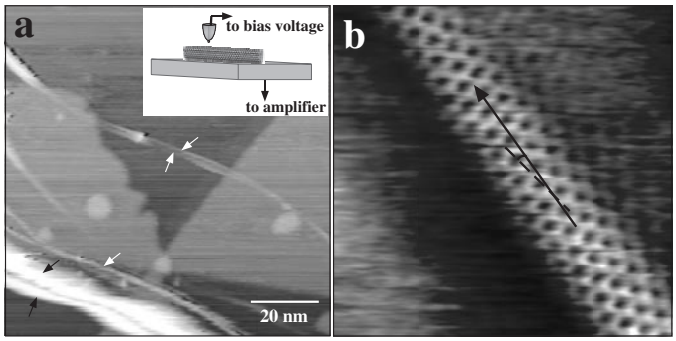

Figure 2. STM images of nanotubes. (*a*) Large area showing several small bundles and isolated SWNTs on a stepped Au(111) surface. The white arrows indicate individual SWNTs and the black arrows point to small ropes of SWNTs. (Inset) schematic diagram of the STM experiment [13]. (*b*) SWNT on the surface of a rope. The solid, black arrow highlights the tube axis and the dashed line indicates the zigzag direction [11].

that some fraction of MWNTs produced by the arc method were semiconducting, and in these semiconducting nanotubes, the STS data suggested that the energy gap depended inversely on diameter. Subsequent STM and STS studies of MWNTs and SWNTs provided indications of different structures and structure-dependent electronic properties, but did not reveal an explicit relationship between structure and electronic properties. The failure of these previous studies to elucidate clearly the expected diameter and helicity dependent electronic properties of nanotubes can be attributed in part to the lack of pure SWNT samples, since (1) the electronic band structure of MWNTs is considerably more complex than SWNTs, and (2) relatively pure samples are required to carry out unambiguous STM and STS measurements.

The development of techniques to produce and purify SWNTs has made possible definitive tests of the predicted electronic properties of nanotubes [19–21]. Indeed, seminal STM and STS measurements of the atomic structure and electronic properties of purified SWNTs by Wildöer *et al* [10] and Odom *et al* [11] have shown that the electronic properties do indeed depend sensitively on diameter and helicity. In both of these studies, the SWNTs were grown by laser vaporization, ultrasonically suspended in organic solvents, and then deposited by spin coating onto Au(111) substrates. Subsequent imaging and spectroscopic studies were carried out at low-temperature, 5 K, in ultra-high vacuum STMs.

2.2. Carbon nanotube atomic structure

A large-scale STM image of individual nanotubes and small ropes containing a number of individual SWNTs is shown in figure 2(*a*). A high-resolution image of a SWNT (figure 2(*b*)) exhibits a graphite-like honeycomb lattice, thus enabling the determination of the (n, m) indices from the image. The (n, m) indices were obtained from the experimentally measured values of the chiral angle and diameter. The chiral angle was measured between the zigzag $(n, 0)$ direction (the dashed line connecting sites separated by 0.426 nm) and the tube axis.

Atomically resolved images of individual SWNTs are shown in figures 3(*a*) and (*b*). The measured chiral angle and diameter of the tube in figure 3(*a*) constrain the (n, m) indices to either (11, 2) or (12, 2). Note that a (11, 2) tube is expected to be metallic, while a (12, 2) tube should be semiconducting. On the other hand, the chiral angle and diameter of the SWNT in figure 3(*b*) constrain the indices to $(14, -3)$. This tube has helicity opposite to the SWNT in figure 3(*a*).

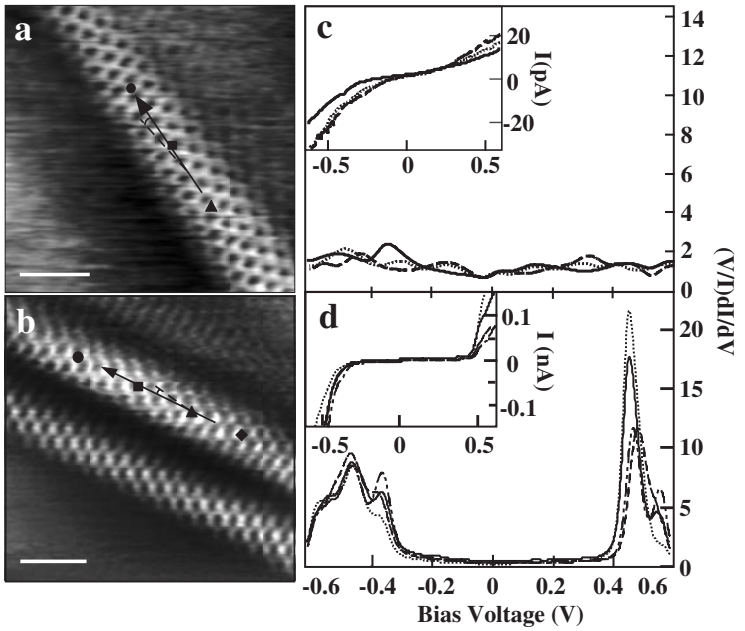

Figure 3. STM imaging and spectroscopy of carbon nanotubes. (*a*), (*b*) Constant current images of SWNTs recorded with bias voltages of 50 and 300 mV, respectively. The solid arrow highlights the tube axis and the dashed curve indicates the zigzag direction. The symbols correspond to positions where I–V curves were recorded. (*c*), (*d*) Calculated normalized conductance $(V/I)\,\mathrm{d}I/\mathrm{d}V$ and measured I–V (inset) recorded at the sites indicated by the symbols in (*a*), (*b*) (adapted from [11]).

2.3. Carbon nanotube electronic structure

Subsequent characterization by tunneling spectroscopy of the atomically resolved tubes can determine whether the electronic properties depend on structure. Tunneling current versus voltage (I–V) data recorded along the two tubes in figure 3 discussed above exhibit very different characteristics (figures 3(*c*) and (*d*)). The normalized conductance, $(V/I)\,\mathrm{d}I/\mathrm{d}V$, which is a good measure of the local density of states (LDOS) [22], from these data sets are quite distinct. For the tube assigned as (11, 2) or (12, 2), the LDOS is finite and constant between -0.6 and +0.6 V. This behavior is characteristic of a metal, and thus shows that the (11, 2) indices provide the best description for the tube. Moreover, the normalized conductance data determined for the (14,$-$3) tube exhibit an absence of electronic states at low energies but sharp increases in the LDOS at -0.325 and +0.425 V. These sharp increases are characteristic of the conduction and valence bands of a semiconductor, and thus confirm the expectation that (14, -3) indices correspond to a semiconducting SWNT. These key measurements first verified the unique ability of SWNTs to exhibit fundamentally different electronic properties with only subtle variations in structure [7–9].

In addition, the semiconducting energy gaps (E_g) of SWNTs are predicted to depend inversely on the tube diameter, d, and to be independent of helicity. A summary of the energy gaps obtained by Odom *et al* [11] for tubes with diameters between 0.7 and 1.1 nm is shown in figure 4.

Significantly, these results and those obtained by Wildöer *et al* [10] for tubes with larger diameters between 1 and 2 nm show the expected $1/d$ dependence. These results can also be used to obtain a value for the nearest neighbor overlap integral ($\gamma_\circ$) used in tight-binding

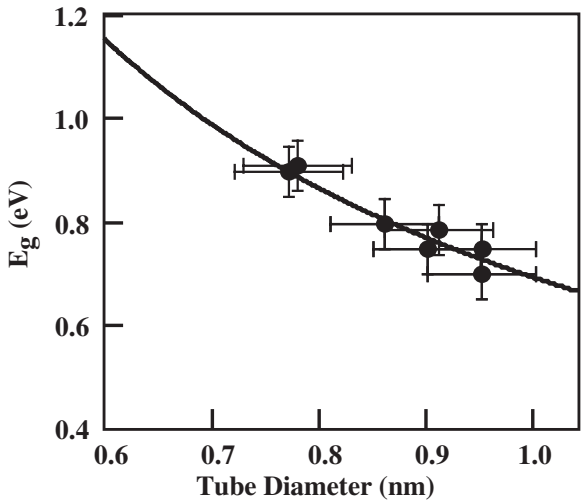

Figure 4. Summary of energy gap (E_g) versus tube diameter obtained in [11]. The solid curve corresponds to a fit described in the text.

calculations of the electronic properties by fitting to $E_g = 2\gamma_\circ a_{C-C}/d$, where a_{C-C} is 0.142 nm. The values obtained from the one parameter fit by [11] and [10] respectively, 2.5 and 2.7 eV, are in good agreement with the reported values in the literature that range from 2.4 to 2.9 eV [1, 23, 24].

2.4. SWNT electronic properties and curvature

The finite curvature of SWNTs should produce small gaps at the Fermi level (E_F) in metallic tubes that depend inversely with the square of their diameter [7, 25]. Although previous STM studies did not observe this small gap structure in chiral (n, m) SWNTs [10, 11], Ouyang *et al* [26] have observed gap-like features near E_F in $(n, 0)$ zigzag tubes (figure 5). Their results confirmed the predicted $1/d^2$ dependence of the curvature-induced gap. In addition, they fit quantitatively the magnitude of these gaps to a model of k_F shifting from $\boldsymbol{K}$, which was found to be consistent with previous tight-binding calculations. The extracted overlap integral value, $\gamma_\circ$, was 2.6 eV, in good agreement with the values obtained in previous STM studies [10, 11].

3. Electronic band structure of carbon nanotubes

The characterization of semiconducting and metallic SWNTs with subtle changes in structure confirms the remarkable electronic behavior of the nanotubes. In addition, the ability to probe simultaneously atomic structure and electronic properties provides an opportunity to investigate further several interesting properties of these 1D materials. These properties include the detailed DOS of the nanotubes and the role of symmetry breaking distortions on the electronic characteristics of the nanotubes.

3.1. One-dimensional electronic structure

Due to the 1D nature of their band structure, SWNTs are expected to exhibit spikes or peaks in their DOS. It is possible to observe these features by extending the energy range

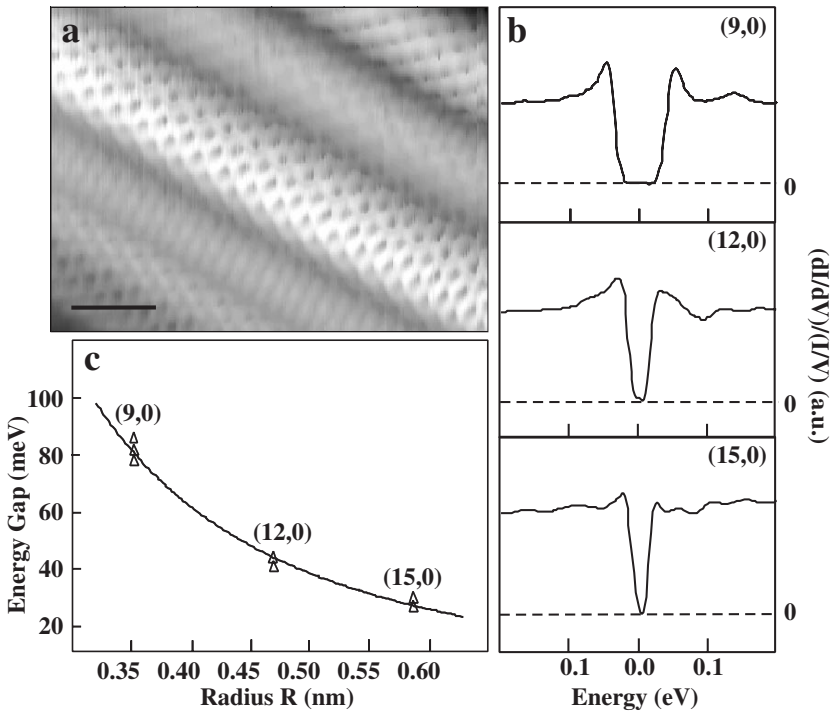

Figure 5. Atomic structure and spectroscopy of zigzag SWNTs. (*a*) STM image of a (15, 0) SWNT exposed on the surface of a rope. Scale bar is 1 nm. (*b*) High-resolution $(V/I)\,\mathrm{d}I/\mathrm{d}V$ calculated from $\mathrm{d}I/\mathrm{d}V$ and I–V images. (*c*) Summary of curvature-induced gaps in metallic zigzag tubes fit to a model that where the gap $\propto 1/d^2$ [26].

at which tunneling spectroscopy measurements are made [10, 27, 28]. When spectroscopic measurements are performed on atomically resolved nanotubes, the experimental DOS can be compared quantitatively with the calculated DOS for specific (n, m) indices. Kim *et al* [28] reported the first detailed experimental comparison with theory on a metallic tube with indices (13, 7). This nanotube is the upper isolated tube that rests on the Au surface shown in figure 6(*a*). The $\mathrm{d}I/\mathrm{d}V$ recorded on this tube (figure 6(*b*)) can be broadly separated into two regions: (1) near E_F, the DOS is finite and constant, and (2) away from E_F, the DOS exhibits a series of sharp peaks that correspond to extremal points in the 1D energy bands.

A comparison of these experimental data to the theoretical band structure calculated by a π-only tight-binding model was made [28]. The spectroscopic data show good agreement with the calculated DOS for the (13, 7) tube (figure 6(*b*)). The agreement between the VHS positions determined from the calculations and $\mathrm{d}I/\mathrm{d}V$ data are especially good below E_F, where the first seven peaks correspond well. The peak splitting due to the anisotropy around $\boldsymbol{K}$ is also reproduced in the $\mathrm{d}I/\mathrm{d}V$. Similar to the expression for the semiconducting energy gap, the experimental 'gap' between the first VHS in metallic tubes is $E_g^m = 6\gamma_\circ a_{C-C}/d$ [29]. The measured value, $E_g^m \sim 1.6$ eV, is in agreement with the predicted value using the measured diameter and $\gamma_\circ = 2.5$ eV, the value determined from the semiconducting energy gap data [11]. Above the Fermi energy some deviation between the experimental data and calculations exists, but the observed differences may be due to band repulsion, which arises from curvature-induced hybridization [30, 31]. Kim *et al* [28] also investigated the sensitivity of the VHS to variations in the (n, m) indices by calculating the DOS of the next closest metallic SWNT; that is, a

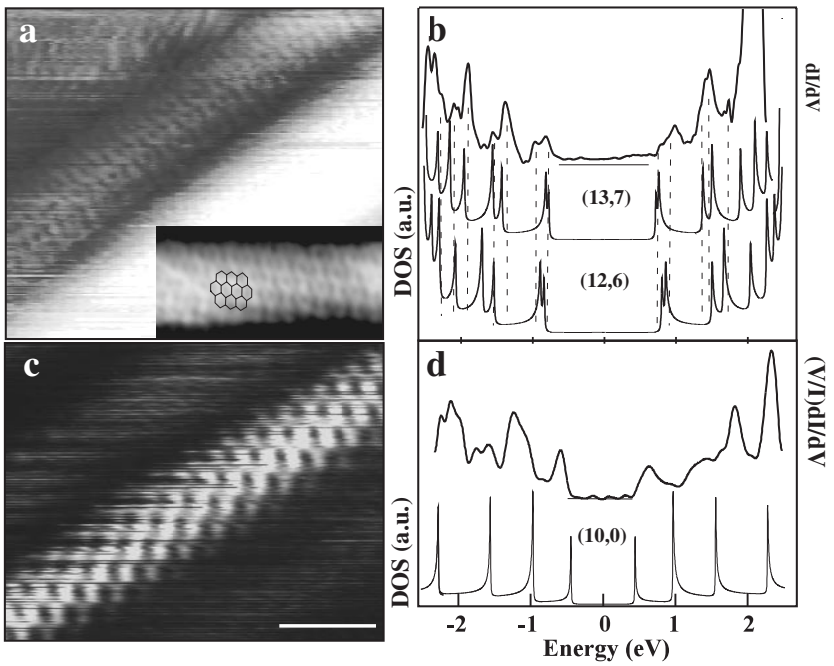

Figure 6. (*a*) Tunneling spectra were recorded on the isolated upper tube. The inset shows an atomic resolution image of this tube. A portion of a hexagonal lattice is overlaid to guide the eye. (*b*) Comparison of the DOS obtained from experiment (upper curve) and a π-only tight-binding calculation for the (13, 7) SWNT (second curve from top). The broken vertical lines indicate the positions of VHS in the tunneling spectra after consideration of thermal broadening convolution. The calculated DOS for a (12, 6) tube is included for comparison [28]. (*c*) Image of a SWNT on the surface of a rope. (*d*) Comparison of the DOS obtained from experiment (upper curve) and calculation for the (10, 0) SWNT (lower curve) [32].

(12, 6) tube. It is worth noting that the poor agreement in this case demonstrates that small variations in diameter and helicity do produce experimentally distinguishable changes in the DOS.

VHS in the electronic DOS of semiconducting nanotubes have also been observed [10,32]. Odom *et al* [32] have characterized spectroscopically a small-diameter (10, 0) semiconducting nanotube (figure 6(*c*)), and directly compared the DOS with a tight-binding calculation for the same indices. The normalized conductance exhibits relatively good agreement with the calculated (10, 0) DOS below E_F but poorer agreement above (figure 6(*d*)). The π-only DOS calculation, however, does not include π/σ and π^*/σ^* mixing due to curvature. This hybridization of π/σ orbitals is believed to produce more pronounced effects on the conduction band [30] than the valence band, and hence might explain the observed deviations. Additional work is needed to resolve this point. Nevertheless, these studies demonstrate that the VHS peaks characteristic of a 1D system can be measured experimentally, and agree well with the DOS calculated using π-only tight-binding models for both semiconducting and metallic nanotubes.

3.2. Symmetry breaking interactions

The experiments described above neglect perturbations to the electronic structure of SWNTs due to interactions with the substrate and other nanotubes. The good agreement between spectroscopic data obtained on isolated tubes and calculations suggest that the substrate does

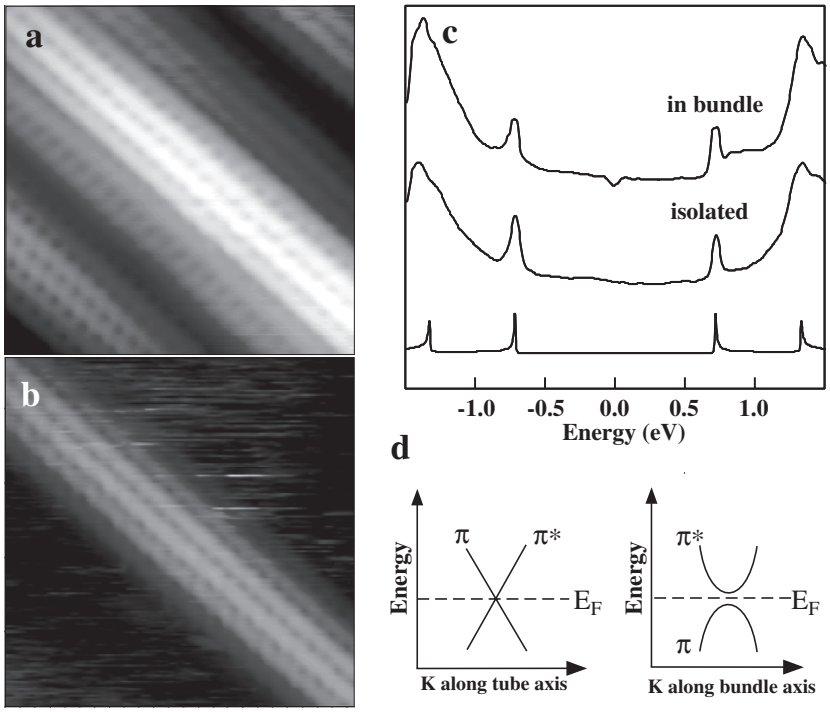

Figure 7. Atomic structure and spectroscopy of armchair SWNTs. (*a*) STM image of an (8, 8) SWNT exposed on the surface of a rope. (*b*) STM image of an (8, 8) SWNT isolated on a Au(111) surface. (*c*) $\mathrm{d}I/\mathrm{d}V$ recorded on the nanotubes in (*a*) and (*b*). The calculated DOS for an isolated (8, 8) tube is displayed below the experimental data [45]. (*d*) (Left) schematic diagram of crossing linear π and π^* bands in an isolated armchair nanotube. (Right) scheme of an avoided crossing of the bands in an armchair nanotube rope which causes a pseudogap in the DOS.

not strongly perturb the band structure. Nanotube–nanotube interactions within a tightly packed rope could, however, modify the electronic properties. Specifically, these intertube interactions can break the rotational symmetry of armchair (n, n) SWNTs, which then allows the π and π^* bands to mix, resulting in a psuedogap at the Fermi energy.

Odom *et al* [32] and Ouyang *et al* [26] have recorded atomically resolved images and spectroscopic data on ropes of armchair (n, n) nanotubes (figure 7(*a*)). The DOS at large energies (about ± 1 eV) exhibit peaks that agree with the positions of the VHS calculated from theory. At energies near E_F, however, a small gap-like feature, $\sim$0.1 eV, is observed. Unlike the curvature-induced gaps in $(n, 0)$ zigzag tubes [26], these gaps have a different shape, and the DOS at E_F is not suppressed to zero. Hence this feature is termed a pseudogap. On (8, 8) armchair tubes isolated on the Au (111) surface (figure 7(*b*)), however, Ouyang *et al* [26] did not observe this psuedogap (figure 7(*c*)).

These observations suggest that the appearance of the pseudogap in armchair tubes arises from interactions with other tubes in the rope. Qualitatively, the origin of this psuedogap can be understood in terms of mixing of the π and π^* bands. In an isolated (n, n) armchair tube, the n-fold mirror planes along the axis prevent the mixing of symmetric (π) and anti-symmetric (π^*). When this rotational symmetry is broken, mixing occurs and a gap (an avoided crossing) occurs (figure 7(*d*)). Ouyang *et al* [26] found that the magnitude of the pseudogaps depends inversely on SWNT radius, which is in qualitative agreement with the predictions by Maarouf *et al* [33].

4. Localized structures and defects in nanotubes

The above results focus on the properties of defect-free, nearly infinite SWNTs. Carbon nanotubes can, however, exhibit a variety of structural defects. For example, the insertion of one or more pentagon–heptagon (five–seven) pairs in the hexagonal network [34, 35] can create intramolecular junctions. In addition, structural deformations such as bends, twisting, and collapse have been observed occasionally in these carbon cylinders [36–38]. These defects may develop during growth, processing, deposition, or following an interaction with surface features [39]. The electronic properties of localized SWNT structures, such as bends and ends [40–42], are essential to proposed device applications. Below, selected examples of structures that have been characterized with atomically resolved imaging and spectroscopy are described.

4.1. Intramolecular junctions

SWNT intramolecular junctions can be formed by interposing one or more pentagon–heptagon pairs in-between two nanotube sections with different (n, m) indices. The resulting morphological change, that is, the angle at which the two nanotube segments join seamlessly, and the electronic nature of the junction, depends on two factors: (1) the number and topological arrangement of the five–seven pairs and (2) the (n, m) indices of each nanotube segment. Theoretical models have predicted that metal–semiconductor (MS), metal–metal (MM), or semiconductor–semiconductor junctions are possible in SWNTs [41, 43, 44].

Ouyang *et al* [45] resolved the atomic structure and electronic properties of two types of junctions, MS and MM. An example of a SWNT intermolecular junction is shown in figure 8(*a*). Noticeably, the center of the junction exhibits a clear perturbation in the regular atomic lattice. Although the upper and lower portions of the nanotube exhibit similiar diameters, 1.57 nm, the chiral angle of each is significantly different, resulting in distinct (n, m) indices. Spectroscopic measurements recorded away from the junction area also revealed that the upper portion of the nanotube is semiconducting with indices $(21, -2)$ and the lower portion is metallic with indices $(22, -5)$ (figure 8(*b*)). Spatially-resolved tunneling spectroscopy indicates that there are no localized states at the interface, which suggests that this MS intramolecular junction can behave as an ideal Schottky diode.

It is difficult to image directly the orientation of multiple five–seven pairs since the defects tend to be distributed along the circumference of the tube, and hence are not accessible by STM imaging. Therefore, Ouyang *et al* [45] compared tight-binding calculations with their spatially resolved spectroscopic measurements in order to determine the most likely configuration of these topological insertions. SWNT segments with the above indices can be seamlessly joined along a common axis using different configurations of five–seven pairs. Tight-binding calculations were performed on nanotube models with the following structure: $(21, -2)|x|(22, -5)$, where x represents a distinct configuration of five–seven pairs. They found that the LDOS calculated from a model with x equaling three separated five–seven pairs best matches their experimental data.

Besides characterizing MS junctions, Ouyang *et al* [45] investigated the properties of an MM junction. Spectroscopic measurements indicate that both nanotube portions are metallic, and unlike the MS junction, show new, low energy features, -0.55 and -0.27 eV, at the junction interface. Similar to the method described above, a model based upon the resolved nanotube was constructed, and the LDOS of the nanotube was calculated at different positions along the tube. These π-only tight-binding calculations were compared with the experimental spectra and were found to agree well with the low energy peak positions and decay length.

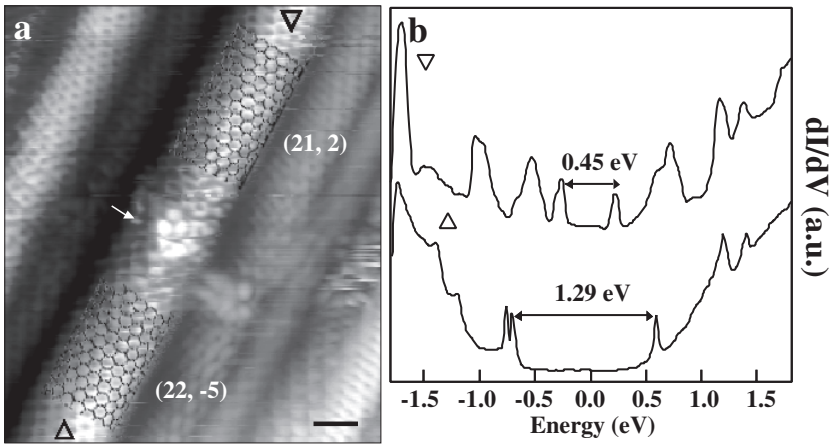

Figure 8. Structure and spectroscopy of a MS intramolecular junction. (*a*) Image of a SWNT containing a junction, whose position is indicated by a white arrow. Black honeycomb meshes are overlaid on the upper and lower portions to highlight the distinct atomic structures. The scale bar is 1 nm. (*b*) Differential conductance $\mathrm{d}I/\mathrm{d}V$ recorded with a lock-in amplifier averaging six sets of raw data. The energy difference between the first VHS gap in the upper semiconducting segment and lower metallic segment are shown [45].

4.2. Bent and twisted nanotubes

Besides lattice defects, mechanical bends and twists can also create changes in the large-scale structure of nanotubes. Odom *et al* [32] reported a bend in an atomically resolved SWNT rope due to a mechanical distortion (figure 9(*a*)). The bend angle defined by this kink was approximately 60°. Tunneling spectroscopy was used to characterize the electronic properties of the uppermost nanotube in the bent rope.

The positions of the van Hove peaks indicate that the tube is metallic. The data also show new features at low bias voltages on either side of the bend. These peaks are likely due to the presence of the bend, since 5 nm away (+) from the kink, the sharpness and prominence of these features have greatly diminished (figure 9(*b*)). In addition, Avouris [47] reported that STS spectra taken near a kink in a semiconducting nanotube also showed an increased DOS at low energies. Notably, recent calculations on bends in armchair tubes show similar low energy features in the DOS for similar bend angles [46] observed by [32] and [47].

The bend region observed by Odom and co-workers was further investigated using bias-dependent STM imaging. On the right side of the bend, a superstructure on the tube is observed at the biases of the localized peaks (figures 9(*c*) and (*d*)). Figure 9(*c*) shows stripes parallel to the zigzag direction of the tube, and figure 9(*d*) displays a triangular ring structure, where the spacing between nearest-neighbor rings is about 0.42 nm (the zigzag spacing). These new electronic features could be due to electron scattering and interference at the defect site [48]. Although the bias voltage, 0.45 V, at which figure 9(*e*) was imaged is not at a prominent peak in the $\mathrm{d}I/\mathrm{d}V$, some electronic structure can be seen extending ∼1.5 nm to the right of the bend. This additional structure, however, diminishes and an unperturbed atomic lattice is observed, consistent with the spectroscopic measurements.

Besides bends in nanotubes, twisting of individual tubes within ropes has been reported by Clauss *et al* [37]. Large-scale nanotube twists may result from mechanical interactions during deposition upon surfaces, be introduced during the growth process and frozen by shear forces, or result from different helicity tubes attempting to align their hexagonal lattices within ropes.

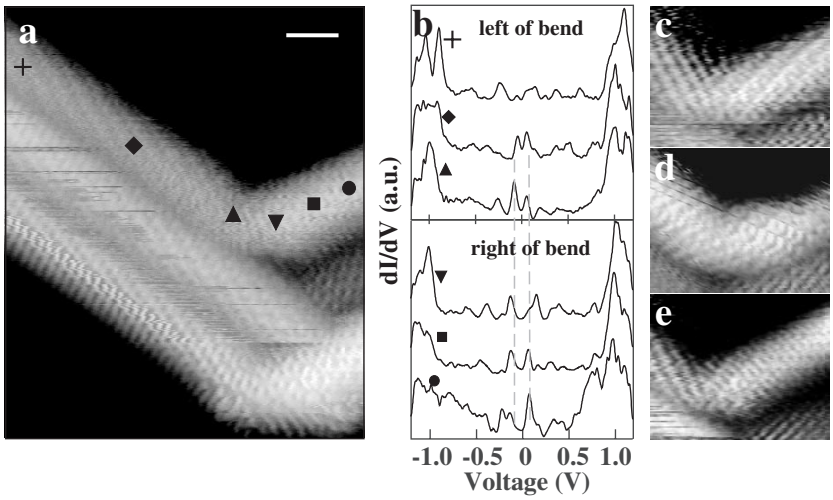

Figure 9. STM image and spectroscopy of a bend in a rope of SWNTs. (*a*) Image of ∼60° bend. The symbols correspond to locations where I–V were measured. The scale bar is 1 nm. (*b*) Differential conductance calculated from the locations indicated in (*a*). The upper portion of the graph is spectroscopy performed on the left side of the bend over 5 nm. The lower portion of the graph is spectroscopy performed on the right side of the bend over 2 nm. The dashed lines highlight the low energy features. (*c*)–(*e*) STM images recorded at bias voltages of −0.15, 0.15, and 0.45 V, respectively [32].

Clauss *et al* [37] observed anomalous lattice orientations upon careful inspection of many tubes, namely, that the armchair direction is on average perpendicular to the tube axis, and that the average angle between the zigzag and armchair direction is greater than 90°. This apparent distortion from an equilibrium conformation can be explained if the imaged nanotubes are of the armchair-type with a twist distortion of several degrees, or from distortions contributed by the finite size and asymmetry of the STM tip.

4.3. Carbon nanotube ends

Another example of localized geometric structures in nanotubes is the ends. Analogous to the surface states of a 3D crystal and the edge state of a 2D electron gas, end states are expected at the end of the 1D electron system. The ends of a 1D electronic system can be considered as the 'surface' of the 1D bulk. Both resonant and localized states are possible at the ends of nanotubes. Resonant end states are expected for metallic nanotubes because there are no gaps in the 1D band structure of metallic SWNTs to localize the end states. In the same way, localized end states are possible for semiconducting nanotubes since they exhibit energy gaps in their DOS.

The end states associated with carbon nanotubes may arise from pentagons in a capped end or an open nanotube [49,50]. In accordance with Euler's rule, a capped end should contain six pentagons. The presence of these topological defects can cause dramatic changes in the LDOS near the end of the nanotube. Kim *et al* [28] reported the first detailed investigation of the electronic character of a capped SWNT end (figure 10) with bulk indices (13, −2). The expected metallic behavior of the (13, −2) tube was confirmed in $(V/I)\,\mathrm{d}I/\mathrm{d}V$ data recorded away from the end (figure 10(*c*)). Spectroscopic data recorded at and close to the SWNT end show two distinct peaks at 250 and 500 mV that decay and eventually disappear in the bulk DOS recorded far from the tube end.

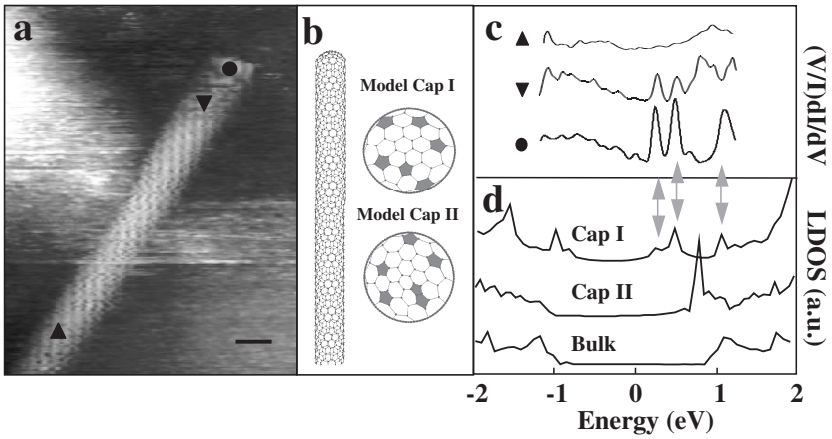

Figure 10. STM image and spectroscopy of a SWNT end. (*a*) Image of a nanotube end. The symbols correspond to the locations where the tunneling spectra in (*c*) were recorded. The scale bar is 1 nm. (*b*) A model (13, −2) SWNT recorded two different cap configurations; the pentagons are shaded gray. (*c*) Experimental tunneling spectra from the end ●, near the end ▼, and far from the end ▲. (*d*) LDOS obtained from tight-binding calculations on capped (13, −2) tubes for caps I and II. Similar features in ● and cap I are highlighted by gray arrows. The bulk DOS for both cap models are identical and is shown in the lowest curve [28].

To investigate the origin of these new spectroscopic features, tight-binding calculations were carried out for a (13, −2) model tube terminated with different end caps (figure 10(*b*)). Both models exhibit a bulk DOS far from the end (lower curve in figure 10(*d*)). Near the nanotube ends, however, the LDOS show pronounced differences from the bulk DOS: two or more peaks appear above E_F, and these peaks decay upon moving away from the end to the bulk. These models were chosen to illustrate the relatively large peak differences for caps closed with isolated versus adjacent pentagons. The LDOS obtained for cap I shows excellent agreement with the measured LDOS at the tube end, while cap II does not (figure 10(*d*)). The positions of the two end LDOS peaks as well as the first band edge of cap I match well with those from the experimental spectra. These results suggest that the arrangement of pentagons is responsible for the observed DOS peaks at the SWNT ends, and are thus similar to conclusions drawn from measurements on MWNTs that were not atomically resolved [50].

Avouris [47] reported spectroscopic data on an atomically-resolved semiconducting SWNT and its end. Interestingly, as tunneling spectra were recorded along the tube axis to the end, the Fermi level position shifted to the center of the energy gap. This is the first reported evidence of band-bending behavior observed by STM spectroscopy in individual nanotubes. Future studies could provide important and much needed information addressing the nature of nanotube–metal contacts.

5. Finite-size effects in SWNTs

The studies reviewed above have focused on SWNTs that retained characteristic features of a periodic 1D system. What happens when this 1D system is made increasingly smaller? Conceptually, as the length of a SWNT is reduced, the end-limit is a fullerene molecular cluster—a 0D object. Investigations of finite-sized SWNTs, therefore, offer an opportunity to probe the connection between and evolution of electronic structure in periodic molecular systems. Studies of finite-size effects in SWNTs are also important to the future utilization of

nanotubes in device applications. Low-temperature transport experiments on metallic SWNTs have shown that μm long tubes behave as islands in single electron transistors, with an island energy level spacing characteristic of the 1D particle-in-a-box states [51, 52]. Since the Coulomb charging energy $E_c \propto 1/L$ (L is the nanotube length), shorter nanotubes allow the working temperature of such devices to increase. Thus at room temperature, if $\Delta E > k_B T$, a resonant tunneling device with nanotube lengths less than 50 nm is possible.

The 1D energy levels and spacing may be described by either quantizing the metallic band structure or by recalling the textbook particle-in-a-box calculation. To first order, the bulk metallic nanotube band structure is characterized by two linear bands (π and π^*) that cross at the Fermi energy. These bands contribute a finite, constant DOS at low energies. Confinement of the electrons due to reduced axial lengths produces a discretization $\Delta k = \pi/L$ on the crossing bands. The intersection of Δk and the linear bands in the zone-folding scheme results in an energy level spectrum. An alternative, simpler analysis of this problem is to consider the finite-length nanotube as a 1D particle-in-a-box, whose well-known eigenvalues (E) are $E = \hbar^2 k^2/2m$. The energy level spacing is easily derived:

$$\Delta E = \hbar^2 k_F \Delta k/m = h v_F/2L \approx 1.67 \text{ eV}/L \text{ (nm)} \tag{3}$$

where h is Planck's constant and $v_F = 8.1 \times 10^5$ m s^{-1} is the Fermi velocity for graphene.

5.1. Quantum effects in carbon nanotubes

STM can in principle probe the transition from 1D delocalized states to molecular levels. Under normal operating conditions, STM can image and record tunneling spectra on the 1D nanotubes. After this characterization, it is then possible to exploit the STM tip to manipulate the nanotubes. Voltage pulses applied between the STM tip and nanotube sample can systematically cut nanotubes into short lengths [32,53] (figure 11(*a*)). Subsequently, these finite-sized nanotubes can be characterized spectroscopically.

Venema *et al* [54] first reported investigations of quantum size effects in a ~30 nm metallic, armchair nanotube shortened by STM voltage pulses. I–V measurements carried out near the middle of the tube showed an irregular step-like behavior. The steps in the spectra observed over a small voltage range ($\pm$0.2 V) correspond to quantized energy levels entering the bias window as the voltage is increased, and the irregularity in the step spacing is due to Coulomb charging effects competing with the 1D level spacing. Remarkably, they discovered that compilation of 100 consecutive I–V measurements (spaced 23 pm apart) into a spectroscopic map exhibited $\mathrm{d}I/\mathrm{d}V$ peaks which varied periodically with position along the tube axis (figure 11(*b*)). This periodic variation in $\mathrm{d}I/\mathrm{d}V$ as a function of position along the tube, ~0.4 nm, is different from the lattice constant $a_\circ = 0.25$ nm (figure 11(*c*)), and can be described by the electronic wavefunctions in the nanotube. Since the $\mathrm{d}I/\mathrm{d}V$ is a measure of the squared amplitude of the wavefunction, they were able to fit the experimental $\mathrm{d}I/\mathrm{d}V$ with the trial function $A \sin^2(2\pi x/\lambda + \phi) + B$. This enabled the separation between the $\mathrm{d}I/\mathrm{d}V$ peaks to be correlated with half the Fermi wavelength λ_F. The calculated value for $\lambda_F = 3a_\circ = 0.74$ nm, determined from the two linear bands crossing at k_F, is in good agreement with experimental observations. Hence discrete electron standing waves were observed in short armchair nanotubes. It is also worth noting that the observed widths of the nanotubes probed in these investigations, ~10 nm, are significantly larger than expected for a single SWNT. This large apparent width suggests that it is likely the measurements were on ropes of SWNTs. In this regard, it will be important in the future to assess how tube–tube interactions perturb the quantum states in a single SWNT.

It is possible that additional features in the electronic structure of finite-sized nanotubes may appear in lengths nearly an order of magnitude shorter. To this end, Odom *et al* [32] have

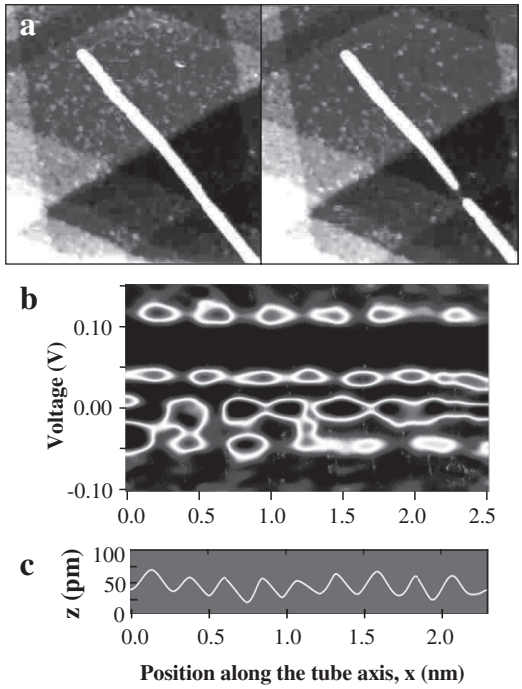

Figure 11. (*a*) SWNTs before and after a voltage pulse was applied to cut the nanotube [53]. (*b*) Spectroscopic image compiled from 100 $\mathrm{d}I/\mathrm{d}V$ measurements. The periodicity is determined from the square of the amplitude of the electron wavefunction at discrete energies. (*c*) Topographic line profile of atomic corrugation in a shortened armchair nanotube [54].

studied quantum size effects in both chiral (n, m) metallic and semiconducting tubes. STM images of nanotubes shortened to 6 and 5 nm are shown in figures 12(*a*) and (*b*), respectively.

The I–V measurements show a step-wise increase of current over a 2-V bias range for both tubes, and the observed peaks in the $(V/I)\,\mathrm{d}I/\mathrm{d}V$ were attributed to resonant tunneling through discrete energy levels resulting from the finite length of the SWNT. Analysis of the peak spacing for the finite-sized nanotubes (figures 12(*d*) and (*e*)) agrees with the simple 1D particle-in-a-box model. The former tube that is 6 nm long exhibits a mean peak spacing of approximately 0.27 eV. A 6 nm tube within this 1D box model would have an average level spacing $\Delta E \sim 1.67\ \mathrm{eV}/6 = 0.28$ eV. For the latter tube with its shorter length, the observed peak spacing is also wider, as expected from this model.

The limitations of this model are evident from the spectroscopic data recorded on a 3 nm-long SWNT (figure 12(*c*)). The $(V/I)\,\mathrm{d}I/\mathrm{d}V$ of this fragment (figure 12(*f*)) appears quite different from the expected $1.67\ \mathrm{eV}/3 = 0.55$ eV energy level spacing for a nanotube 3 nm long. In a top-down approach, *ab initio* calculations have shown that the energy level spacing of finite-sized tubes may be considerably different from that predicted from a Hückel model due to the asymmetry and shifting of the linear bands crossing at E_F [55]. From a bottom-up approach, several molecular computational studies have predicted that nanotubes less than 4 nm long should open a HOMO–LUMO gap around E_F, although its magnitude varies greatly among different calculation methods [56, 57]. These studies have been performed on finite-sized, open-ended, achiral $(n, 0)$ zigzag and (n, n) armchair tubes. It is evident that these ultra-short length scales in nanotubes offer an opportunity for different computational methods to complement each other.

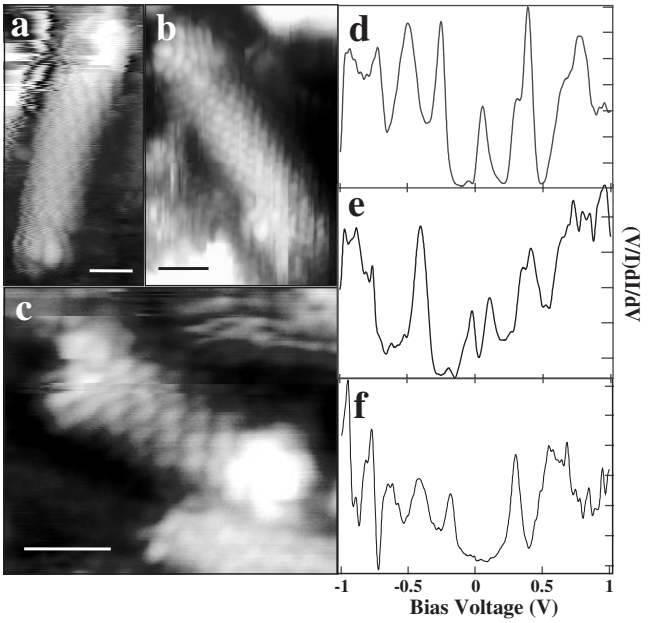

Figure 12. STM imaging and spectroscopy of finite-sized SWNTs. (*a*)–(*c*) SWNTs cut by voltage pulses and shortened to lengths of 6, 5, and 3 nm, respectively. (*d*)–(*f*) Averaged normalized conductance recorded on the nanotubes in (*a*)–(*c*), respectively [32].

In contrast to the metallic nanotubes, no significant length dependence is observed in finite-sized semiconducting nanotubes down to 5 nm (figure 13) [58]. Namely, tunneling spectroscopy data obtained from the center of the shortened tubes showed a striking resemblance to the spectra observed before cutting. That is, the positions of the valence and conduction bands are nearly identical before and after cutting (figures 13(*b*) and (*d*)) for both 20 and 5 nm tube lengths. Spectra taken at the ends also exhibited the same VHS positions, and a localized state near ∼0.2 eV, which is attributed to dangling bonds, was also observed. It is possible that long-length scale disorder and very short electron mean free paths (∼2 nm) in semiconducting tubes [59] may account for the similar electronic behavior observed in short and long nanotubes. This suggests that detailed studies should be carried out with even shorter tube lengths. However, *ab initio* calculations on the electronic structure of semiconducting nanotubes with lengths of 2–3 nm also seem robust to reduced-length effects and merely reproduce the major features of the bulk DOS (i.e. the energy gap) [60].

5.2. Coulomb charging in carbon nanotubes

In the previous experiments on shortened nanotubes, the finite-sized nanotubes remained in good contact with the underlying substrate after cutting, and hence the voltage drop was primarily over the vacuum tunnel junction. If the nanotubes are weakly coupled to the surface, a second barrier for electron tunneling is created, and the nanotube fragments may behave as Coulomb islands and exhibit Coulomb blockade and staircase features in their I–V [61]. The investigation of finite-sized nanotubes in the presence of charging effects is interesting since both effects scale inversely with length L, in contrast to 3D metal quantum dots [62, 63].

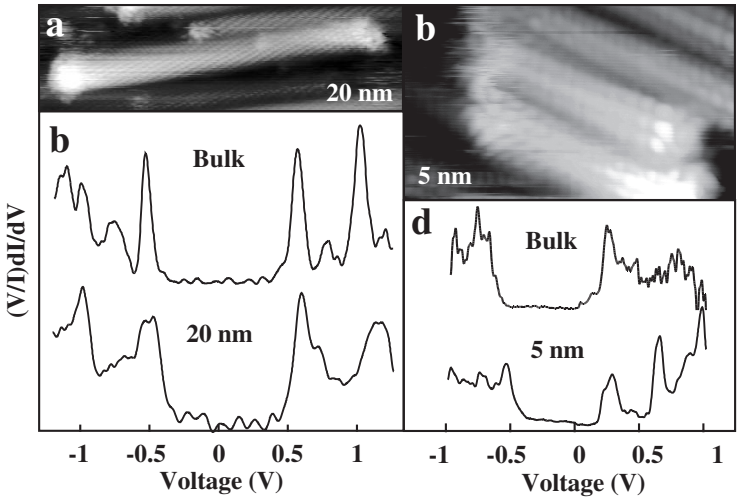

Figure 13. (*a*) STM image of a semiconducting SWNT shortened to 20 nm. (*b*) Comparison of the normalized conductance for the tube in (*a*) and the uncut tube prior to cutting. The spectra are nearly identical. (*c*) STM image of a SWNT shortened to 5 nm. (*d*) Comparison of the normalized conductance for the tube in (*c*) and the uncut tube prior to cutting.

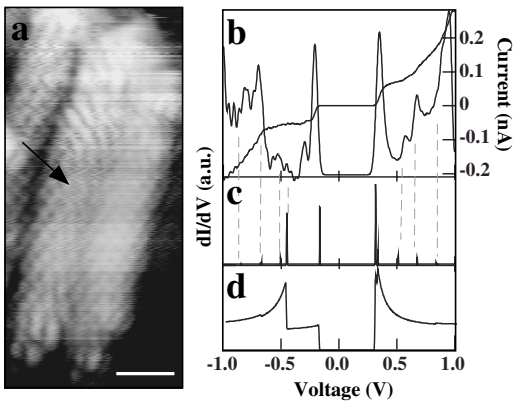

Figure 14. Charging effects in finite-sized SWNTs. (*a*) STM image of SWNTs shortened by voltage pulses. The scale bar is 1 nm. (*b*) Measured I–V and $\mathrm{d}I/\mathrm{d}V$ performed on the tube indicated by an arrow in (*a*). (*c*) Numerical derivative of the I–V curve calculated by a semi-classical calculation including the level spacing of a 1D box. (*d*) Same calculation as in (*c*) except the nanotube DOS is treated as continuous [32].

Odom *et al* [32] reported the first detailed investigation of the interplay between these two effects in nanotubes at ultra-short length scales and compared the tunneling spectra with a modified semi-classical theory for single-electron tunneling. The I–V of the nanotube in figure 14(*a*) exhibits a suppression of current at zero bias as well as relatively sharp, irregular step-like increases at larger $|V|$ (figure 14(*b*)), reminiscent of the Coulomb blockade and staircase [61]. Similar to [54], the irregularities in the conductance peak spacing and amplitude are attributed to contributions from the discrete level spacing of the finite-sized nanotube [32].

To compare directly the complex tunneling spectra with calculations, Odom *et al* [32] modified a semi-classical double junction model [62] to include the level spacing of the

nanotube quantum dot, $\Delta E \sim 1.67$ eV$/7 = 0.24$ eV. The capacitance of a SWNT resting on a metal surface may be approximated by [64]

$$C = 2\pi\varepsilon L/\ln[d_z + (d_z^2 - R^2)^{1/2}]/R \tag{4}$$

where d_z is the distance from the center of the nanotube to the surface, and ε is 8.85×10^{-3} aF nm^{-1}. Estimating $d_z \sim 1.9$ nm, the geometric capacitance for the nanotube in figure 14(*a*) is 0.21 aF. The calculated $\mathrm{d}I/\mathrm{d}V$ that best fits the tunneling conductance is shown in figure 14(*c*), and yields a Au-tube capacitance $C_1 = 0.21 \pm 0.01$ aF, in good agreement with the capacitance estimated by the geometry of the nanotube. In contrast, if the calculation neglected the level spacing of the nanotube island, only the blockade region is reproduced well (figure 14(*d*)). These studies demonstrate that it is possible to study the interplay between finite-size effects and charging effects in SWNT quantum dots.

6. Magnetic impurity effects on SWNTs

This review will now shift gears to describe how the electronic structure of SWNTs is affected by external perturbations, namely, magnetic impurities. These studies are important for investigating new physical phenomenon as well as for determining the robustness of a nanotube's intrinsic properties in the presence of impurities.

6.1. STM and the Kondo effect

The interaction between the magnetic moment of a magnetic impurity atom and the conduction electron spins of a non-magnetic host, the Kondo effect, is a well-known phenomena that leads to anomalous transport measurements in bulk systems of dilute magnetic alloys [65]. For temperatures below the Kondo temperature (T_K), the electrons of the host screen the local spin of the impurity, and the result is the emergence of a Kondo resonance. This resonance should disappear at temperatures above T_K. A magnetic nanostructure comprised of a magnetic impurity and a carbon nanotube host is an interesting system since the impurity spins would interact with conduction electrons confined to one-dimension, and in addition, might potentially spin-couple to a strongly (versus weakly) interacting electron system [66].

In the STM experiments described above, an electron tunnels directly from the STM tip to the nanotube sample. With magnetic impurities deposited on the sample, two different paths are now available for the electrons to tunnel from the tip: (1) to the localized orbital of the magnetic impurity and (2) to the continuous electron states of the nanotube. Because the final state of the electron can occupy two energetically degenerate possible states, this can lead to quantum interference. This interference produces narrow features in the tunneling spectra near E_F above the magnetic center. The resonance lineshape is a reflection of how much the impurity orbitals contribute to the tunneling probability, and in Fano's model [67], is quantified by the interference parameter q. A symmetric anti-resonance occurs when the tunneling transition probability to the localized state is very small ($q = 0$). An increased tunneling transition probability to the discrete state ($q \sim 1$) results in an asymmetric lineshape, and in the case where tunneling to the impurity channel dominates the continuum one ($q > 1$), the resonance approaches the Breit–Wigner shape.

6.2. Magnetic impurities in a 1D electron system

Odom *et al* [68] decorated individual SWNTs with well-separated, about 1 nm, Co clusters (figure 15(*a*)). The spectroscopic data recorded on the bare nanotube 7 nm away from the Co is

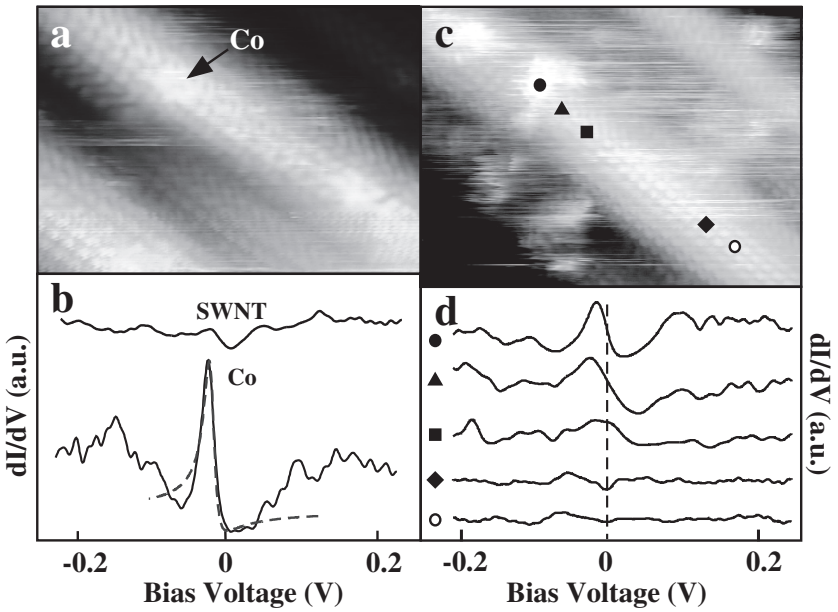

Figure 15. (*a*) STM image of 0.5 nm Co clusters situated on individual SWNTs. (*b*) Differential conductance, $\mathrm{d}I/\mathrm{d}V$, calculated from I–V curves taken over the bare nanotube ∼7 nm away from the Co, and above the Co cluster in (*a*). The feature identified as a Kondo resonance appears over the Co. The dashed line indicates a fit to a theory explained in detail in [70]. (*c*) STM image of slightly larger Co clusters <1 nm situated on resolved carbon nanotubes. (*d*) $\mathrm{d}I/\mathrm{d}V$ as a function of position along the tube in (*c*) (indicated by the symbols ●, ▲, ■, ♦, ○), starting with I–V performed over the cluster (●). The effect of the Co on the nanotube spectra has nearly disappeared after 2 nm (adapted from [68]).

finite and nearly constant over the small bias range, consistent with the nanotube being metallic (figure 15(*b*)). In contrast, the $\mathrm{d}I/\mathrm{d}V$ spectrum taken directly above the 0.5 nm Co center shows a strong resonance peak near E_F, $V = 0$. This spectroscopic feature was observed above ten different small Co clusters (<1 nm) situated on metallic nanotubes, and is strongly suggestive of the presence of a Kondo resonance in the 1D SWNTs [68].

In addition, Odom *et al* [68] performed spatially resolved tunneling measurements to characterize the length scale over which the impurity influenced the nanotube's electronic spectrum. Spectroscopic data obtained for a 0.7 nm wide Co cluster on an atomically resolved metallic SWNT (figure 15(*c*)) are shown in figure 15(*d*). At the center of the Co site, the resonance feature exhibits a peak structure similar in shape but slightly broader than the peak in figure 15(*b*). The peak feature systematically decreases in amplitude in spectra recorded at increasing distances from the Co center. The sharp resonance disappears completely after ∼2 nm. This decay length is similar to, although slightly longer than, that reported for Co atoms on either Au(111) or Cu(111) surfaces [69, 70].

To verify that the prominent spectroscopic resonances were due to the interaction of the magnetic Co with the metallic SWNTs, a number of control experiments were carried out. First, the measurements were repeated with non-magnetic Ag clusters on SWNTs, and indeed, no peak feature was observed near E_F due to the small Ag cluster. This result demonstrates unambiguously that the presence of the magnetic Co cluster is critical to observe the resonance, and that the observed peak feature is not simply an enhancement in the local DOS due to

a metallic cluster. Second, spectroscopic measurements were performed over Co clusters supported by intrinsic semiconducting SWNTs, and these spectra did not exhibit any new features at E_F. This observation suggested that the peak feature at E_F is not due to the bare Co d-orbital resonance and emphasized the necessity of conduction electrons in the host to interact with the magnetic cluster in order to observe the Kondo resonance.

The resonance lineshape observed over small Co clusters was fit to a modified Anderson single-impurity model [70]. The dashed curve in figure 15(*b*) shows a relatively good fit to the data taken above the center of the Co center. The fit reveals that the Kondo temperature for the Co/SWNT system is ∼90 K, confirming that the measurements at 5 K were made in the $T < T_K$ limit. To examine the validity of this prediction for T_K, the measurements were repeated at 80 K. Significantly, no peaks were found in $\mathrm{d}I/\mathrm{d}V$ over Co sites situated on metallic SWNTs. Hence, this observation is consistent with the predicted value of T_K, although the disappearance occurs at a temperature approximately 10 K lower than obtained from the fit. Moreover, the Kondo temperature for the Co/SWNT system from these STM experiments is similar to the value extracted by thermopower measurements on SWNT mats doped with various transition metal catalysts [71].

The localization of the d-orbitals of a magnetic impurity in its conduction electron host is reflected in the lineshape of the Kondo resonance, whose overall lineshape is governed by the magnitude of the Fano parameter q. From the theoretical fit in figure 15(*b*), $|q|$ is 2.7; in general, for the Co/SWNT system, q falls in a range $2.7 \leqslant |q| \leqslant 3.3$. These large values of q (> 1) indicate that the transition probability to tunnel into the localized d-orbital of the Co cluster is large compared to the π-electron continuum of the carbon nanotube. In contrast, q values reported for magnetic impurities on 2D noble metal surfaces were relatively small (0–0.7), and the Kondo resonance was observed as a dip or anti-resonance in the $\mathrm{d}I/\mathrm{d}V$. It is possible that these differences originate from the detailed characteristics of the non-magnetic host, and may be due to differences between the delocalization of p-orbitals on carbon and those on noble metal surfaces or a reduction in the number of available final states in the 1D SWNT.

6.3. Magnetic impurities in a SWNT quantum box

Perhaps the ultimate magnetic nanostructure is a magnetic atom in a quantum box. Odom *et al* [68] created such nanostructures by the cutting method described earlier, and characterized spectroscopically Co on SWNTs before and after manipulating the nanotube length. The familiar Kondo resonance is observed near $V = 0$ in the $\mathrm{d}I/\mathrm{d}V$ for spectra taken above a Co cluster situated on an uncut metallic SWNT (figure 16(*a*)). An atomically resolved 11 nm nanotube segment created by applying voltage pulses on each side of the Co cluster is shown in figure 16(*b*). Spectroscopic data recorded over the Co site (figure 16(*c*)) exhibit an average level spacing of ∼0.15 eV, in agreement with the length-dependent level spacing discussed above. Notably, the peak amplitude at E_F appears significantly enhanced relative to the other energy level peaks. To investigate the origin of this increased conductance, they characterized the level structure near E_F versus distance from the cluster (figure 16(*d*)). The amplitude of this central peak at E_F decreases over the same length scale, 2 nm, as the Kondo resonance decays from a Co cluster along an extended 1D SWNT, although the amplitude of peaks at $E \neq E_F$ are similar. The enhanced conductance at E_F provides evidence of the sensitivity of the electronic properties of metallic nanotubes to magnetic impurities, even in finite-sized structures.

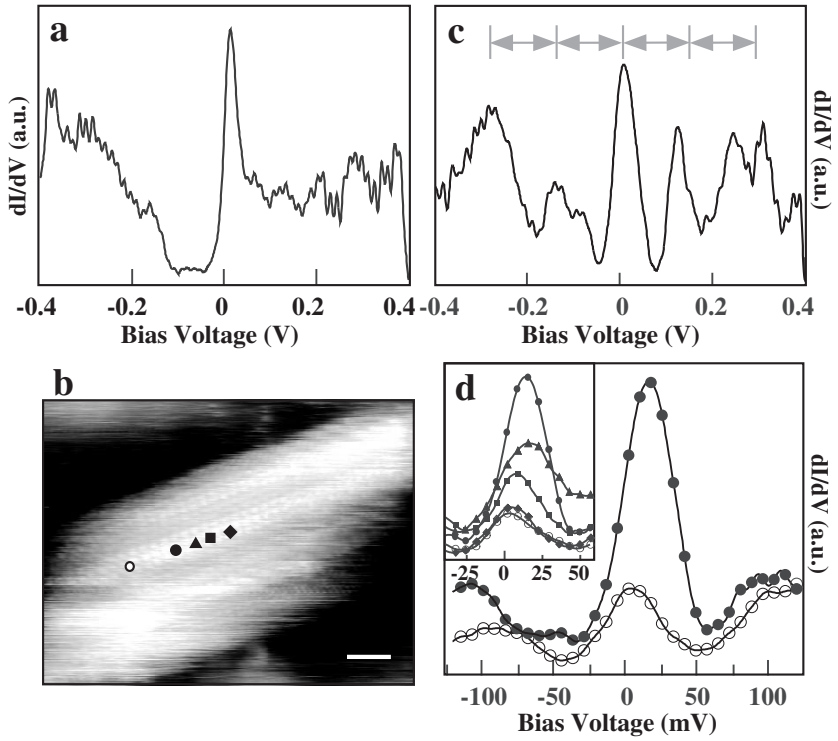

Figure 16. (*a*) $\mathrm{d}I/\mathrm{d}V$ spectrum recorded at the site of a small Co cluster on a long nanotube. (*b*) Atomically resolved image of the nanotube shortened to 11 nm. The symbols ●, ▲, ■, ♦, ○ indicate the positions at which I–V curves were taken, and the filled black circle (●) highlights the position of the cluster. The scale bar corresponds to 1 nm. (*c*) $\mathrm{d}I/\mathrm{d}V$ results obtained at the position of the small Co cluster in (*b*). (*d*) Comparison of the peak amplitude near E_F recorded at the Co cluster (●) and about 1.5 nm away (○). (Inset) $\mathrm{d}I/\mathrm{d}V$ data recorded at the positions indicated in (*a*). Adapted from [68].

7. Conclusions and future directions

STS has been used to characterize the atomic structure and tunneling density of states of individual SWNTs and SWNT ropes. Defect-free SWNTs exhibit semiconducting and metallic behavior that depends predictably on the chiral angle and diameter. In addition, the 1D VHS in the DOS for both metallic and semiconducting tubes have been characterized and compare well with tight-binding calculations. Using STM as a tool to create finite-sized SWNTs, it has been possible to access a regime of '0D' behavior, where finite length produces quantization along the tube axis. This work opens up future opportunities to probe, for example, connections between extended and molecular systems and to explore possible device applications. Lastly, metallic nanotubes decorated with magnetic impurities exhibit an enhancement in their conductance at low energies, and unique applications of these magnetic nanostructures may soon be uncovered. In short, much of the fascinating overall structural and electronic properties of SWNTs are now in hand—but this has really only scratched the surface. Future work addressing the role of defects and other structural perturbations, coupling to metallic and magnetic systems, the connection between extended and finite size/molecular clusters, as well as other directions will help to define further the fundamental physics of these systems and define emerging concepts in nanotechnology.

References

[1] Dresselhaus M S and Dresselhaus G 1996 *Science of Fullerenes and Carbon Nanotubes* (San Diego: Academic)
[2] Yakobson B I and Smalley R E 1997 *Am. Sci.* **85** 324
[3] Dekker C 1999 *Phys. Today* **52** 22
[4] Treacy M M J, Ebbesen T W and Gibson J M 1996 *Nature* **381** 678
[5] Wong E W, Sheehan P E and Lieber C M 1997 *Science* **277** 1971
[6] Yakobson B I, Brabec C J and Bernholc J 1996 *Phys. Rev. Lett.* **76** 251
[7] Hamada N, Sawada S and Oshiyama A 1992 *Phys. Rev. Lett.* **68** 1579
[8] Mintmire J W, Dunlap B I and White C T 1992 *Phys. Rev. Lett.* **68** 631
[9] Saito R, Fujita M, Dresselhaus G and Dresselhaus M S 1992 *Appl. Phys. Lett.* **60** 2204
[10] Wildöer J W G, Venema L C, Rinzler A G, Smalley R E and Dekker C 1998 *Nature* **391** 59
[11] Odom T W, Huang J L, Kim P and Lieber C M 1998 *Nature* **391** 62
[12] Lieber C M 1998 *Solid State Commun.* **107** 607
[13] Hu J T, Odom T W and Lieber C M 1999 *Acc. Chem. Res.* **32** 435
[14] Kane C L and Mele E J 1997 *Phys. Rev. Lett.* **78** 1932
[15] Crespi V H, Cohen M L and Rubio A 1997 *Phys. Rev. Lett.* **79** 2093
[16] Ge M and Sattler K 1993 *Science* **260** 515
[17] Zhang Z and Lieber C M 1993 *Appl. Phys. Lett.* **62** 2972
[18] Olk C H and Heremans J P 1994 *J. Mater. Res.* **9** 259
[19] Thess A *et al* 1996 *Science* **273** 483
[20] Journet C, Maser W K, Bernier P, Loiseau A, Lamy de la Chapelle M, Lefrant S, Deniard P, Lee R and Fischer J E 1997 *Nature* **388** 756
[21] Guo G, Nikolaev P, Thess A, Colbert D T and Smalley R E 1995 *Chem. Phys. Lett.* **243** 49
[22] Stoisco J A and Feenstra R M 1993 *Scanning Tunneling Microscopy* (New York: Academic)
[23] White C T and Mintmire J W 1998 *Nature* **394** 29
[24] White C T, Robertson D H and Mintmire J W 1993 *Phys. Rev.* B **47** 5485
[25] Saito R, Fujita M, Dresselhaus G and Dresselhaus M S 1992 *Phys. Rev.* B **46** 1804
[26] Ouyang M, Huang J L, Cheung C L and Lieber C M 2001 *Science* **292** 702
[27] Odom T W, Huang J L, Kim P, Ouyang M and Lieber C M 1998 *J. Mater. Res.* **13** 2380
[28] Kim P, Odom T W, Huang J L and Lieber C M 1999 *Phys. Rev. Lett.* **82** 1225
[29] Rubio A 1999 *Appl. Phys. A. Mater.* **68** 275
[30] Blasé X, Benedict L X, Shirley E L and Louie S G 1994 *Phys. Rev. Lett.* **72** 1878
[31] Charlier J C and Lambin Ph 1998 *Phys. Rev.* B **57** R15 037
[32] Odom T W, Huang J L, Kim P and Lieber C M 2000 *J. Phys. Chem.* B **104** 2794
[33] Maarouf A A, Kane C and Mele E J 2000 *Phys. Rev.* B **61** 11 156
[34] Meunier V, Henrard L and Lambin Ph 1998 *Phys. Rev.* B **57** 2596
[35] Charlier J C, Ebbeson T W and Lambin Ph 1996 *Phys. Rev.* B **53** 11 108
[36] Hertel T, Walkup R E and Avouris Ph 1998 *Phys. Rev.* B **58** 13 870
[37] Clauss W, Bergeron D J and Johnson A T 1998 *Phys. Rev.* B **58** 4266
[38] Chopra N G, Benedict L X, Crespi V H, Cohen M L, Louie S G and Zettl A 1995 *Nature* **377** 135
[39] Lambin P, Meunier V and Biro L P 1998 *Carbon* **36** 701
[40] Lambin P, Lucas A A and Charlier J C 1997 *J. Phys. Chem. Solids* **58** 1833
[41] Chico L, Crespi V H, Benedict L X, Louie S G and Cohen M L 1996 *Phys. Rev. Lett.* **76** 971
[42] Han J, Anantram M P, Jaffe R L, Kong J and Dai H 1998 *Phys. Rev.* B **57** 14 983
[43] Charlier J C, Ebbesen T W and Lambin P 1996 *Phys. Rev.* B **53** 11 108
[44] Saito R, Dresselhaus G and Dresselhaus M S 1996 *Phys. Rev.* B **53** 2044
[45] Ouyang M, Huang J L, Cheung C L and Lieber C M 2001 *Science* **291** 97
[46] Rochefort A, Salahub D R and Avouris P 1998 *Chem. Phys. Lett.* **297** 45
[47] Avouris P, Martel R, Ikeda H, Hersam M, Shea H R and Rochefort A 2000 *Science and Applications of Nanotubes* ed D Tomanek and R J Enbody (New York: Kluwer) pp 223–37
[48] Kane C L and Mele E J 1999 *Phys. Rev.* B **59** R12 759
[49] Tamura R and Tsukada M 1995 *Phys. Rev.* B **52** 6015
[50] Carroll D L, Redlich P, Ajayan P M, Charlier J C, Blasé X, DeVita A and Car R 1997 *Phys. Rev. Lett.* **78** 2811
[51] Bockrath M, Cobden D H, McEuen P L, Chopra N G, Zettl A, Thess A and Smalley R E 1997 *Science* **275** 1922
[52] Tans S J, Devoret M H, Dai H, Thess A, Smalley R E, Geerligs L J and Dekker C 1997 *Nature* **386** 474
[53] Venema L C, Wildoer J W G, Temminck Tunistra H L J, Dekker C, Rinzler A and Smalley R E 1997 *Appl. Phys. Lett.* **71** 2629

[54] Venema L C, Wildoer J W G, Janssen J W, Tans S J, Temminck Tuinstra H L J, Kouwenhoven L P and Dekker C 1999 *Science* **283** 52
[55] Rubio A, Sanchez-Portal D, Attach E, Ordoejon P and Soler J M 1999 *Phys. Rev. Lett.* **82** 3520
[56] Bulusheva L G, Okotrub A V, Romanov D A and Tomanek D 1998 *J. Phys. Chem.* A **102** 975
[57] Rochefort A, Salahub D R and Avouris P 1999 *J. Phys. Chem.* B **103** 641
[58] Odom T W, Hafner J H and Lieber C M 2001 *Carbon Nanotubes, Top. Appl. Phys.* **80** 173
[59] McEuen P L, Bockrath M, Cobden D H, Yoon Y G and Louie S G 1999 *Phys. Rev. Lett.* **83** 5098
[60] Jishi R A, Bragin J and Lou L 1999 *Phys. Rev.* B **59** 9862
[61] Grabert H and Devoret M H 1992 *Single Charge Tunneling* (New York: Plenum)
[62] Hanna A E and Tinkham M 1991 *Phys. Rev.* B **44** 5919
[63] Ralph D C, Black C T and Tinkham M 1995 *Phys. Rev. Lett.* **74** 3241
[64] Nayfeh M H and Brussel M K 1985 *Electricity and Magnetism* (New York: Wiley)
[65] Kondo J 1964 *Prog. Theor. Phys.* **32** 37
[66] Bockrath M, Cobden D H, Lu J, Rinzler A G, Smalley R E, Balents T and McEuen P L 1999 *Nature* **397** 598
[67] Fano U 1961 *Phys. Rev.* **124** 1866
[68] Odom T W, Huang J L, Cheung C L and Lieber C M 2000 *Science* **290** 1549
[69] Li J, Schneider W D, Berndt R and Delley B 1998 *Phys. Rev. Lett.* **80** 2893
[70] Madhavan V, Chen W, Jamneala T, Crommie M F and Wingreen N S 1998 *Science* **280** 567
[71] Grigorian L and Eklund P 1999 *Phys. Rev.* B **60** R11 309